Electronic Properties of Anthracene Derivatives for Blue Light Emitting Electroluminescent Layers in Organic Light Emitting Diodes: A Density Functional Theory Study†

P. Raghunath,‡ M. Ananth Reddy,‡,§ C. Gouri,# K. Bhanuprakash,*,‡ and V. Jayathirtha Rao*,§

Inorganic Chemistry Division and Organic Chemistry Division (II), Indian Institute of Chemical Technology, Hyderabad 500 007, India, and PSC Division, Vikram Sarabhai Space Centre, Thiruvanthapuram 695 022, India

Received: September 30, 2005; In Final Form: November 9, 2005

Molecular level parameters are investigated computationally to understand the factors that are responsible for the higher efficiency in derivatives of 9,10-bis(1-naphthyl)anthracene (α-ADN), 9,10-bis(2-naphthyl)anthracene (β-ADN), their tetramethyl derivatives (α,β-TMADN) and the *t*-Bu derivative (β-TBADN) as blue light emitting electroluminescent (EL) layers in organic light emitting diodes (OLEDs). DFT studies at the B3LYP/6-31G-(d,p) level have been carried out on the substituted anthracenes. The absorption spectra are simulated using time dependent DFT methods (TD-DFT) whereas the emission spectra are approximated by optimizing the excited state by HF/CI-Singles and then carrying out the vertical CI calculations by the TD-DFT method. The reorganization energy for estimating the hole and electron transport is calculated. The transfer integrals between parallely stacked molecules in the bulk state are estimated by calculating the electronic splitting. The substituted anthracenes are compared with unsubstituted anthracene and yet untested 9,10-dianthrylanthracene (TANTH). A larger and slower buildup of the electrons and holes in the EL layer, due to the higher reorganization energy and smaller electronic coupling between the adjacent molecules could lead to an increase in hole−electron recombination in the layer and thus increase the efficiency.

Introduction

Organic π-conjugated materials with semiconducting properties have attracted immense interest from both the scientific community and industrialists because of their potential applications as active elements in light-emitting diodes (LED).[1−5] These materials offer certain advantages over the standard/existing inorganic materials for use in LEDs, such as versatility of chemical synthesis, low cost, ease of processing, flexibility, excellent color gamut and high fluorescence efficiency. Moreover, white-light emission from an LED is possible from organic materials only. The optoelectronic properties of organic LEDs (OLEDs) depend on several factors.[6−9] Among these, the important parameters pertaining to the organic materials used in them are the appropriate HOMO and LUMO energy levels for the electroluminescence layer (ELL), hole transport layer (HTL) and electron transport layer (ETL), suitable electron and hole mobility in these layers, the geometrical characteristics of molecules leading to the favored packing patterns, and the intermolecular interactions. The hetero-junction HTL/ELL should be designed to facilitate hole injection from the HTL into the ELL and to block electron injection, if any, back into the HTL. This necessitates that the HOMO of the HTL should be matching with that of the ELL (so that holes can readily enter the ELL) and that the LUMO of ELL should be significantly below the HTL (to prevent electrons entering the HTL). The ETL/ELL hetero-junction should be designed to facilitate electron injection into the ELL and to block holes, if any, entering the ETL. For this, the LUMO of the ELL should be matching with that of the ETL (for easy flow of electrons to the ELL) and the HOMO of the ETL should be significantly below that of the ELL (to prevent holes flowing into the ETL) (Scheme 1). Thus, by selecting molecules with appropriate HOMO and LUMO levels, charge carriers can be made to flow into the ELL from the opposite directions. In addition, the mobility of the charges in the ELL should be good enough for their efficient transport through the layer; at the same time, it should not be too high to allow them cross over to the next layers. This situation leads to the concentration of holes and electrons in ELL, exciton formation, and fluorescence from the ELL. The mobility/transport properties of the charges in the organic molecules are dependent on their reorganization energies (λ), and the coupling between the molecules packed in the solid state is dependent on the electron-transfer coupling matrix element, *t*.[6−9] The charge-transfer processes are very much influenced by the geometry and molecular packing of atoms in the molecules as well as by the intermolecular interaction parameters. Thus, it follows that a proper understanding of all these molecular characteristics of the organic materials used in OLEDs is an important prerequisite for the design and selection

SCHEME 1: Hole and Electron Recombination in the EL Layer

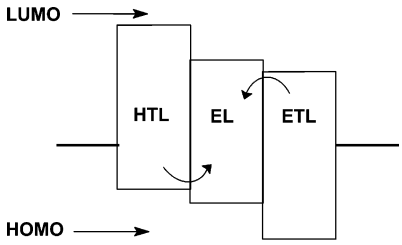

† IICT Communication number: 051206/CMM0010.

* Corresponding author. E-mail: bhanu2505@yahoo.co.in.
‡ Inorganic Chemistry Division, Indian Institute of Chemical Technology.
§ Organic Chemistry Division (II), Indian Institute of Chemical Technology.
# Vikram Sarabhai Space Centre.

10.1021/jp0555753 CCC: $33.50
Published on Web 12/27/2005

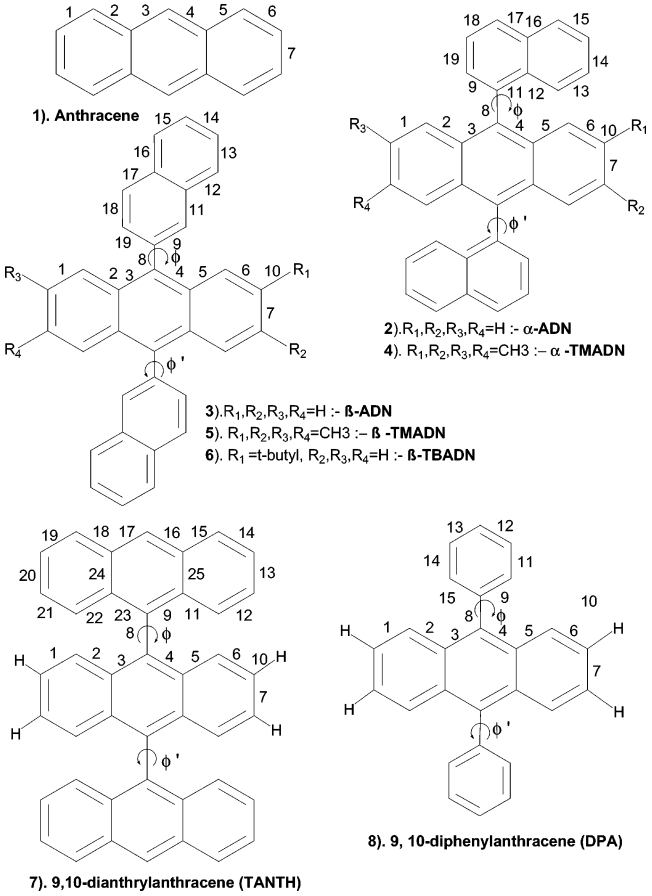

Figure 1. Molecular structures and bond numbering scheme used for Anthracene, α-ADN, *β*-ADN, α-TMADN, *β*-TMADN and *β*-TBADN, DPA, and TANTH.

of appropriate molecules as well as for optimizing the performance of the devices. Here quantum chemical studies of these molecular properties have proven to be invaluable and been shown to be of immense help in designing and improving the devices.[10−15]

Many emitting materials have been designed and used in OLEDs; however, high-performance, blue-light emitting ones are rare, because of the intrinsic wide band-gap required for such materials. Many hole transporting materials have been tried for blue emission.[1−5] Anthracene derivatives form an important class of highly efficient, stable, blue-light emitting materials.[16−21] It has been suggested that nonplanar derivatives of anthracene, due to steric factors may hinder close packing and improve the device performance; hence the EL anthracene derivatives have been designed solely on the basis of this principle. Among them the 9,10-disubstituted compounds (shown in Figure 1) such as 9,10-diphenylanthracene (DPA), 9,10-dinaphthylanthracene (ADN) (both α and *β* forms), 2-*tert*-butyl ADN (*β*-TBADN) and tetramethyl ADN (both α and *β*-TMADN) have been studied for their performance and found to be efficient materials for full color OLED display devices.[16−21] *β*-ADN, as the emitter, was suggested by Shi and Tang, and they found that the device structure NPB/ADN/ Alq3 produced a good efficiency of 1.9 cd/A.[16] As ADN proved to be morphologically unstable due to crystallizations, substitutions to this molecule like methyl in the fourth position were carried out.[17,18] But here for a similar device structure the efficiency dropped to 1.4 cd/A. On the other hand, both in ADN and in methyl substituted ADN upon doping there was an increase in the efficiency. Very recently, Kan et al. reported two blue-emitting isomers of TMADN with excellent color purity and high efficiency.[19] The hole transport layer was the *N*,*N*′-biphenyl-*N*,*N*′-bis(1-naphthyl)[1,1′-biphenyl]-4,4′-diamine (NPB) and the electron transport 4,7-diphenyl-1,10-phenanthroline (BPhen). The HOMO−LUMO gap and the emission spectra of these two emitters are nearly same but the *β* form shows a larger efficiency of 4.5 cd/A when compared to the 3.1 cd/A for the α isomer. Employing a blend (doping) of α- and *β*-TMADN in a 9:1 weight ratio as the EL layer in the OLED, Kan et al. could fabricate an OLED with a blue emission of higher brightness and efficiency, compared to that of the α or *β* forms when used alone in the device. It was suggested that the large energy barrier between the HOMO energy levels of the TMADN and that of BPhen effectively blocked the holes from transferring from the EL layer to the ET layer, thus confining the hole and electron combination to the EL layer, but no explanation was offered for the better performance of the *β* isomer.[19] The different behaviors of the two isomers in the same device with the same HOMO, LUMO levels and HOMO−LUMO gap suggest that some other molecular level parameters may also be playing a role in enhancing the efficiency. This also suggests that a fine-tuning of the luminous efficiency of anthracene derivatives is possible.

Although literature is abundant with the computational studies on *π*-conjugated organic materials, those addressing the issues related to the efficiencies of the EL of such materials are few.[22,23] Moreover, the molecular parameters of these materials play a decisive role in contributing to their high efficiencies. In this study, we have carried out a detailed DFT analysis of the selected 9,10-disubstituted anthracene derivatives. This consists of geometry optimization of the neutral molecules, their cations and anions, leading to the information on their molecular geometries, optical absorption characteristics and HOMO, LUMO levels. Calculation of reorganization energies to estimate the hole and electron transport properties in these molecules are also carried out. Electronic splitting (2t) of the HOMO and LUMO levels as a function of distance between adjacent molecules is calculated to estimate the transfer integrals.

On the basis of the molecular level parameters, we analyze the performance of substituted anthracenes comparing them with unsubstituted anthracene. We also include a yet untested anthracene derivative, namely 9,10-dianthrylanthracene, and evaluate the efficiency on the basis of the obtained data. We find that this molecule does not have the same molecular parameters as the other substituted ones. This detailed study presented here should be helpful in understanding and designing efficient anthracene based EL.

Computational Methods

For this study we have chosen seven derivatives of anthracene along with the basic anthracene moiety for comparison and these structures are shown in Figure 1. The aryl substitutions in general are in the 9 and 10 position of the anthracene ring. Molecule **1** is the unsubstituted anthracene moiety and **2** is 9,10-bis(1-naphthyl)anthracene (α-ADN) and **3** is 9,10-bis(2-naphthyl)anthracene (*β*-ADN). These two isomers defer in the connectivity; in the α isomer the naphthalene connects to the anthracene through its 1 position whereas in the *β* isomer the connection is through the 2 position. Molecules **4** and **5** (α-TMADN and *β*-TMADN) are the tetramethyl-substituted forms (2, 3, 6, and 7 substituted) of **2** and **3**. Molecule **6** is the 2-*tert*-butyl-9,10-bis(2-naphthyl)anthracene which is a derivative of the *β* form and will be referred to as *β*-TBADN. Molecule **7** (TANTH) is 9,10-dianthrylanthracene or trisanthracane and molecule **8** is the diphenylanthracene derivative (DPA). All these

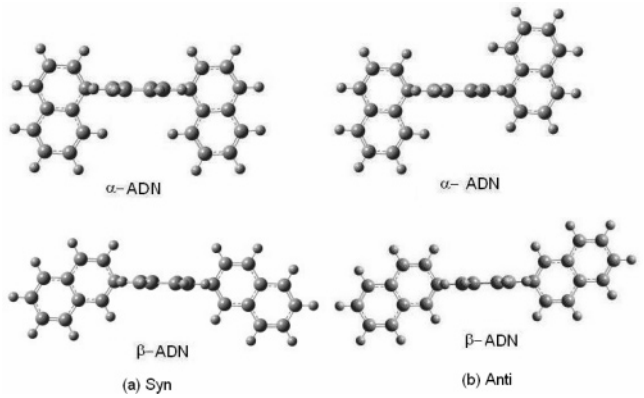

Figure 2. Syn (a) and anti (b) conformations of α- and *β*-ADN.

TABLE 1: Dihedral Angles (*ϕ*, deg) Obtained at Various Minima for the Neutral, Cation and Anions Calculated at the B3LYP/6-31G(d,p) Level[a,b]

molecule	neutral	cation	anion
α-ADN	90	90 and 68.5 (C_2)	90 and 69.7 (C_2)
β-ADN	90 and 76.3 (C_2)	90 and 57.9 (C_2)	90 and 55.6 (C_2)
α-TMADN	90	90 and 72.7 (C_2)	90 and 68.8 (C_2)
β-TMADN	90 and 80.6 (C_2)	90 and 60.9 (C_2)	90 and 54.2 (C_2)
β-TBADN[c]	87 (C_1)	61.2 (C_1)	59.6 (C_1)
TANTH	90	90 and 77.8 (C_2)	90 and 83 (C_2)
DPA	90 and 83.9 (C_1)	90 and 61.5 (D_2)	90 and 60.2 (D_2)

[a] Almost equal angles are obtained for both syn and anti conformations. Only the syn conformation is shown in the table. [b] All molecules with 90° angles are in C_{2v} symmetry. Other symmetries are indicated in parentheses. [c] $\phi' = 78.2°$ (neutral), 59.6° (cation) and 57.9° (anion).

derivatives except TANTH have been studied as EL for blue light emission.[16−21]

We have carried out the geometry optimization of all the neutral molecules shown in the figure using the G03w software.[24] The minimization is carried using the density functional theory at the B3LYP level. The B3LYP functional consists of Becke's three-parameter hybrid exchange functional combined with the Lee−Yang−Parr correlation functional.[25,26] The basis set used is a split valence plus polarization, 6-31G(d,p). Frequency calculations are carried out to ensure that each optimized conformation has all positive frequencies and thus is a minimum on the potential energy surface. MP2/6-31G(d,p) calculations have been carried out on some neutral molecules to verify the stationary points obtained at the B3LYP level. The excitation energies of the low lying excited states have been calculated using the time dependent density functional theory (TD-DFT) also available as an option in the G03w suite of programs.[27,28] The emission properties is approximated by optimizing the first excited state using the HF/configuration interaction singles (CIS) methodology[29a] and then subsequently using this geometry for the TD-DFT calculations. This method has shown to be ideal in estimating emission spectra and further details are available in the literature.[30]

The main parameters for hole/electron transport at the molecular level are the reorganization energies due to the oxidation and reduction of the molecule and the electronic splitting between adjacent molecules (transfer integrals). To study the reorganization energies, the knowledge of the optimized geometry of the cation and the anion is necessary and this is obtained by the open shell calculations of the molecules at the UB3LYP/6-31G(d,p) level. For the transfer integral evaluation, the single point calculations of the neutral dimers are carried out at the B3LYP/6-31G(d,p) geometry using the semiempirical intermediate neglect of differential overlap (INDO) Hamiltonian.[29b]

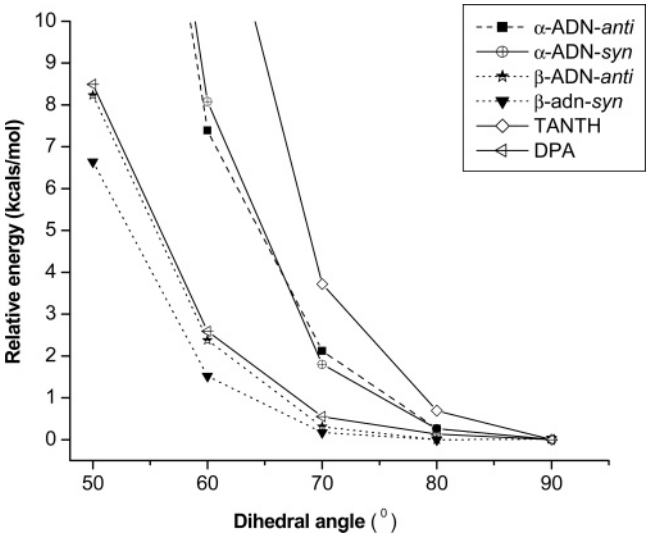

Figure 3. Change in energy with dihedral angle *ϕ* for the neutral molecules calculated at B3LYP/6-31G(d,p) single point level.

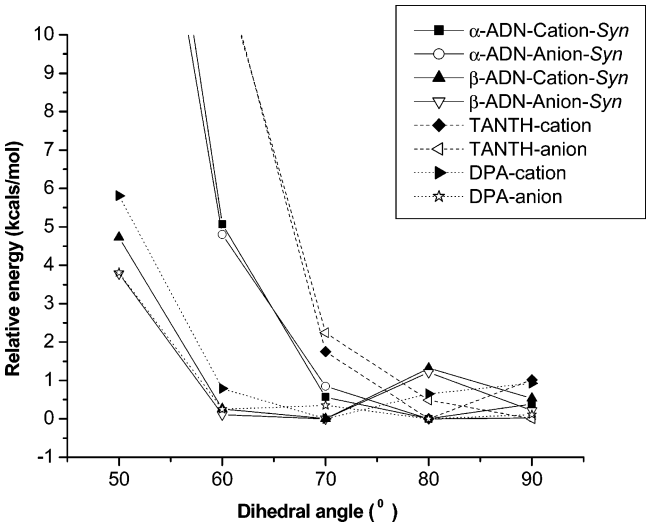

Figure 4. Change in energy with dihedral angle *ϕ* for the cation and anion molecules calculated at UB3LYP/6-31G(d,p) single point level.

Results and Discussion

(1) Conformations and Relative Energy. It is observed, from the 3-D structures of these molecules, except in the case of unsubstituted anthracene all other molecules show conformational flexibility. For the α,*β*-ADN, α,*β*-TMADN and *β*-TBADN molecules due to the presence of the side groups, we obtain two nearly degenerate conformations as shown in Figure 2 for α,*β*-ADN only: when the two side groups are on the same side, a syn conformation (a), and when they are on the opposite side, an anti conformation (b). These are not interconvertible by rotation of the side groups due to steric hindrances at smaller torsion angles, *ϕ*. In the case of DPA and TANTH we obtain only one conformation due to symmetry. Apart from TBADN, the molecules in general prefer a more symmetric structure with the angles *ϕ* and *ϕ*′ on both sides being equal.

Due to the rotational freedom in the side groups attached to the anthracene, we can envisage many local minima at larger *ϕ* in both conformations in the gas phase which can get locked in

TABLE 2: Comparison of the Bond Lengths (Å) Obtained at the B3LYP/6-31G(d,p) Level for the Neutral, Cation, and Anions of α,β-ADN and α,β-TMADN[a]

	α-ADN (β-ADN)[b]					α-TMADN (β-TMADN)[b]				
	neutral[c]	cation		anion		neutral[c]	cation		anion	
bond	90°	90°	68.5° (57.9°)	90°	69.7°(55.6°)	90°	90°	72.7° (60.9°)	90°	68.8° (54.2°)
1	1.369 (1.369)	1.388 (1.389)	1.384 (1.384)	1.392 (1.392)	1.389 (1.384)	1.372 (1.372)	1.392 (1.392)	1.390 (1.389)	1.395 (1.395)	1.390 (1.386)
2	1.433 (1.433)	1.416 (1.416)	1.420 (1.420)	1.420 (1.420)	1.422 (1.424)	1.431 (1.430)	1.415 (1.415)	1.417 (1.417)	1.418 (1.419)	1.420 (1.423)
3	1.412 (1.412)	1.425 (1.425)	1.426 (1.429)	1.428 (1.426)	1.431 (1.433)	1.412 (1.411)	1.423 (1.423)	1.424 (1.428)	1.428 (1.426)	1.431 (1.433)
4	1.412 (1.412)	1.425 (1.425)	1.429 (1.431)	1.428 (1.426)	1.430 (1.433)	1.412 (1.411)	1.423 (1.423)	1.426 (1.429)	1.428 (1.426)	1.430 (1.433)
5	1.433 (1.433)	1.416 (1.416)	1.418 (1.419)	1.421 (1.421)	1.422 (1.425)	1.431 (1.430)	1.415 (1.415)	1.415 (1.416)	1.418 (1.419)	1.420 (1.423)
6	1.369 (1.369)	1.388 (1.389)	1.385 (1.384)	1.392 (1.392)	1.388 (1.384)	1.372 (1.372)	1.392 (1.393)	1.390 (1.390)	1.395 (1.393)	1.390 (1.386)
7	1.422 (1.422)	1.403 (1.403)	1.405 (1.404)	1.400 (1.400)	1.402 (1.405)	1.441 (1.441)	1.423 (1.423)	1.424 (1.423)	1.413 (1.413)	1.417 (1.419)
8	1.500 (1.498)	1.494 (1.492)	1.486 (1.478)	1.495 (1.494)	1.491 (1.480)	1.499 (1.498)	1.494 (1.493)	1.490 (1.482)	1.495 (1.493)	1.489 (1.478)
9	1.383 (1.382)	1.384 (1.383)	1.391 (1.393)	1.386 (1.384)	1.390 (1.395)	1.383 (1.382)	1.384 (1.383)	1.387 (1.390)	1.386 (1.384)	1.391 (1.396)
10						1.509 (1.508)	1.504 (1.504)	1.505 (1.505)	1.511 (1.511)	1.511 (1.510)
11	1.435 (1.420)	1.434 (1.420)	1.438 (1.415)	1.439 (1.421)	1.422 (1.417)	1.435 (1.421)	1.434 (1.420)	1.436 (1.416)	1.439 (1.420)	1.443 (1.417)
12	1.422 (1.421)	1.422 (1.421)	1.421 (1.422)	1.422 (1.422)	1.421 (1.424)	1.422 (1.421)	1.422 (1.421)	1.422 (1.422)	1.422 (1.422)	1.421 (1.424)
13	1.376 (1.376)	1.377 (1.376)	1.378 (1.376)	1.377 (1.377)	1.378 (1.380)	1.376 (1.376)	1.377 (1.376)	1.377 (1.376)	1.377 (1.377)	1.378 (1.380)
14	1.415 (1.417)	1.415 (1.417)	1.414 (1.416)	1.416 (1.417)	1.415 (1.413)	1.415 (1.417)	1.415 (1.417)	1.414 (1.416)	1.416 (1.417)	1.414 (1.413)
15	1.375 (1.376)	1.375 (1.376)	1.376 (1.379)	1.376 (1.377)	1.376 (1.383)	1.375 (1.376)	1.375 (1.376)	1.376 (1.378)	1.376 (1.377)	1.377 (1.384)
16	1.421 (1.421)	1.421 (1.420)	1.420 (1.416)	1.422 (1.420)	1.422 (1.415)	1.421 (1.420)	1.421 (1.420)	1.421 (1.418)	1.422 (1.420)	1.422 (1.415)
17	1.420 (1.420)	1.420 (1.420)	1.419 (1.423)	1.420 (1.420)	1.419 (1.424)	1.420 (1.420)	1.420 (1.420)	1.420 (1.422)	1.420 (1.420)	1.419 (1.425)
18	1.375 (1.375)	1.375 (1.376)	1.377 (1.373)	1.375 (1.376)	1.378 (1.373)	1.375 (1.375)	1.375 (1.376)	1.376 (1.373)	1.375 (1.376)	1.379 (1.373)
19	1.415 (1.424)	1.414 (1.425)	1.409 (1.428)	1.415 (1.428)	1.411 (1.432)	1.415 (1.425)	1.414 (1.425)	1.412 (1.428)	1.415 (1.428)	1.410 (1.432)

[a] For cation and anion both minima are shown. [b] Values given in parentheses correspond to the β isomer. [c] For the neutral only the minima at 90° is shown. See text for details.

TABLE 3: Optimized Bond Lengths (Å) for the Neutral, Cation, and Anions of β-TBADN, TANTH, DPA, and Anthracene Obtained at the B3LYP/6-31G(d,p) Level

	β-TBADN			TANTH					DPA					anthracene		
	neutral	cation	anion	anion	cation		anion		neutral	cation		anion		neutral	cation	anion
bond	78°	59.8°	5.6°	90°	90°	77°	90°	83°	90°	90°	61.5°	90°	60.2°			
1	1.369	1.384	1.384	1.369	1.369	1.375	1.369	1.375	1.369	1.389	1.387	1.392	1.389	1.370	1.391	1.395
2	1.433	1.42	1.424	1.433	1.433	1.426	1.433	1.429	1.433	1.416	1.418	1.421	1.422	1.430	1.414	1.419
3	1.413	1.43	1.433	1.413	1.412	1.421	1.414	1.419	1.418	1.424	1.429	1.426	1.433	1.400	1.410	1.414
4	1.412	1.43	1.432	1.413	1.412	1.421	1.414	1.419	1.412	1.424	1.429	1.426	1.432	1.400	1.410	1.414
5	1.434	1.419	1.426	1.433	1.432	1.426	1.433	1.429	1.433	1.416	1.418	1.421	1.422	1.430	1.414	1.419
6	1.373	1.393	1.389	1.369	1.369	1.375	1.369	1.375	1.369	1.389	1.387	1.392	1.389	1.370	1.391	1.395
7	1.433	1.416	1.414	1.422	1.422	1.415	1.423	1.417	1.422	1.403	1.403	1.400	1.400	1.426	1.405	1.403
8	1.497	1.480	1.479	1.501	1.499	1.493	1.500	1.498	1.498	1.492	1.482	1.495	1.486			
9	1.382	1.391	1.394	1.415	1.421	1.422	1.422	1.423	1.403	1.403	1.408	1.405	1.411			
10	1.537	1.534	1.417													
11	1.421	1.416	1.539	1.432	1.424	1.427	1.426	1.427	1.396	1.395	1.393	1.396	1.394			
12	1.421	1.422	1.424	1.370	1.380	1.376	1.382	1.379	1.396	1.396	1.397	1.396	1.397			
13	1.376	1.376	1.379	1.424	1.414	1.418	1.413	1.416	1.396	1.396	1.397	1.396	1.397			
14	1.416	1.416	1.413	1.368	1.378	1.374	1.380	1.377	1.396	1.395	1.393	1.396	1.394			
15	1.376	1.379	1.383	1.430	1.423	1.426	1.425	1.426	1.403	1.403	1.408	1.406	1.411			
16	1.420	1.417	1.415	1.398	1.402	1.400	1.404	1.403								
17	1.420	1.422	1.425	1.398	1.402	1.400	1.404	1.403								
18	1.375	1.373	1.373	1.430	1.423	1.426	1.425	1.426								
19	1.425	1.428	1.432	1.368	1.378	1.374	1.380	1.377								
20				1.424	1.414	1.418	1.413	1.416								
21				1.370	1.380	1.376	1.382	1.379								
22				1.432	1.424	1.427	1.426	1.427								
23				1.415	1.421	1.422	1.422	1.423								
24				1.446	1.443	1.444	1.448	1.448								
25				1.446	1.443	1.444	1.448	1.448								

the solid state due to crystal forces. Geometric optimization of all the neutral molecules at the B3LYP/6-31G(d,p) level reveals that except for TBADN all the other substituted anthracenes show a minima at $\phi = 90.0°$. Earlier studies using higher level models such as CASSCF indicate that phenylanthracene, a similar type of molecule, also has a minimum at 90.0°.[31] This 90.0° angle is expected as it has the minimum steric interactions, and this is irrespective of the conformation (syn and anti). We confirm this minima by carrying out additional calculations at the MP2/6-31G(d,p) level for all the neutral molecules. In the case of β isomers additional local minima are also seen. These minima have a relative energy difference of hardly 0.5 kcal/mol and there is practically no change in the bond lengths or the bond angles in both the middle anthracene ring and the side rings. We shall show in a later section that there is no difference in the HOMO, LUMO orbital energies, or in the absorption and emission values with the change in dihedral angle unless it takes up very small values. Hence for all further discussions and calculations we shall refer to the 90.0° dihedral angle as the minimum. The dihedral angles obtained for neutral, cation and anion at the local minima are tabulated in Table 1. To estimate the energy required for the symmetric rotation ($\phi = \phi'$) from these local minima for the two conformations and the two isomers (α and β), we plot the relative energy calculated for various angles vs the torsion angle and this is shown in Figure 3. Here the syn and anti neutral molecules of only α,β-ADN

TABLE 4: HOMO, LUMO, and HOMO−LUMO Gap (HLG, eV), Wavelength (λ_{max}, nm), Excitation Energy (ΔE, eV), Oscillator Strength (f), Ground State Dipole Moments (μ_g, Debye), Contributing Transitions and Transition Dipole Moments (Debye) for All Molecules[a]

						absorption data				
molecule	sym	HOMO (eV)	LUMO (eV)	HLG (eV)	μ_g (D)	λ_{max} (nm)	ΔE (eV)	f	transition	transition dipole (D)
anthracene	D_{2h}	−5.22	−1.63	3.59	0.0	379	3.27	0.06	H → L (0.64) H−1 → L+1(0.1)	0.86
α-ADN[b]	C_{2v}	−5.15	−1.66	3.49	0.0	394	3.15	0.18	H → L (0.64)	1.51
β-ADN[b]	C_{2v}	−5.13	−1.63	3.50	0.05	395	3.16	0.21	H → L (0.64)	1.66
α-TMADN[b]	C_{2v}	−4.91	−1.41	3.50	0.06	394	3.14	0.15	H → L (0.64)	1.38
β-TMADN[b]	C_{2v}	−4.89	−1.39	3.50	0.01	393	3.15	0.18	H → L (0.64)	1.52
β-TBADN[b]	C_1	−5.04	−1.55	3.48	0.52	398 (396)[c]	3.12	0.23	H → L (0.64)	1.70
DPA	C_{2v}	−5.11	−1.61	3.50	0.0	391	3.17	0.15	H → L (0.64) H−1 → L+1 (0.01)	1.37
TANTH	C_{2v}	−5.18	−1.70	3.48	0.0	403	3.08	0.37	H → L (0.52) H−1 → L+2 (0.27) H−2 → L+1 (0.27)	2.23

[a] Absorption data obtained using TD-DFT method for the B3LYP/6-31G(d,p) level optimized geometries. [b] Syn conformation only. [c] Experimental value.[18,21]

are shown for comparison. It is interesting to observe that for the β isomer the energy required for the rotation is less than 1 kcal/mol between the angles 90° and 70° for both conformations whereas for both the α isomer conformations such a low energy rotation is seen only between 90° and 80° (a smaller range). Below 80°, the energy of the α isomer rises up very steeply when compared to the β isomer where the rise below 70° is much slower. This also indicates that in the neutral species the steric hindrances in the α isomers are much larger and in the solid state there exists a possibility that the β isomer can take lower torsion angles. From the graph it is also clear that both the syn and anti conformations of the ADN derivatives behave in a similar fashion; henceforth we tabulate and discuss the results of only the syn isomer for clarity. We also observe (Table 1) that there is no major notable change in ϕ in the isomers, which have been substituted by alkyl groups as in α,β-TMADN, hence these are not shown. In Figure 4 where only the syn conformers have been shown, it is seen that this low energy rotation in these two ADN isomers is not observed in the oxidized and the reduced state (cation and the anion). Geometrical optimization of the cation and the anion reveal that deeper local minima occur at the lower angles.

As the neutral has almost low energy rotation for the range 70−90° (β) and 80−90° (α) in the gas phase, we can only predict the angle range (each molecule could have different angle) it can take up in the solid state rather than one particular angle. Crystal forces then lock any angle taken up by the molecule in the solid state. Angle ϕ for the molecule is not predicted to be outside the range due to steric factors. However, in the case of the cation and the anion a relatively deeper minima occurs around 70° for α and around 60° for β in addition to the 90° minima. As the difference in bond lengths in both the minima are seen to be larger in the case of cation and anion (Table 2), we shall discuss the results in terms of both minima in these cases unlike in the neutral one.

In Figure 3 the variation of neutral TANTH and DPA with respect to the torsion angle is also shown for comparison. Here in the case of DPA the rotation is almost similar to the case of β isomer. Two crystal structures reported in the literature indicate the torsion angles as 69° in one case and 67° in another.[32,33] But in TANTH the steric factors start even at 80°, and there is a steep rise in the curve from that angle. In Figure 4, potential energy surface (PES) of the cation and the anion of these molecules are shown and these also behave similarly. A deviation in behavior is seen in case of syn β-TBADN where ϕ is not equal to 90° due to the bulky group in one position. For the neutral we obtain around 87° and for the cation/anion 61.2°/59.6° (Table 1). Summarizing, we find that the larger the steric interactions (due to the ring size), smaller the angle range for low energy rotation.

(2) Bond Lengths. The DFT/B3LYP-6-31G(d,p) minimized bond lengths for all the molecules are shown in Tables 2 and 3. The numbering scheme used for the bonds, is shown in Figure 1. To understand the effect of substitution of the four-methyl groups on the neutral α and the β forms of ADN, we compare the bond lengths with those of the corresponding TMADN. It is seen that there is almost no change in the bond lengths both in the anthracene part and in the naphthalene part except in case of bond 7 (and its equivalent bond due to symmetry). In this bond there is a lengthening of almost 0.02 Å in TMADN, which we attribute to the steric interactions of the methyl groups. It has already been pointed out in the earlier section that the torsion angle between the anthracene and naphthalene does not change much with substitutions on the anthracene ring and we find it is also the case in the length of the connecting bond 8. On comparing the α and the β isomers of ADN and TMADN, we again find that the anthracene does not have any substantial bond length change. But in the naphthalene bonds 11 and 19, which are adjacent to the connecting bonds, have a considerable change of around 0.015 Å, whereas all the other bond lengths in the side rings also remain almost the same. This is expected and this change is attributed to the change in connectivity (1 and 2 position of the naphthalene).

On oxidation/reduction of each molecule to the corresponding cation/anion, more interesting changes in the bond lengths take place. First there is a substantial change in the bond length in bond 8, which is the connecting bond between the anthracene and the naphthalene ring. This bond shortens by 0.005−0.006 Å in the cation when the torsion angle is 90° but shortens further by 0.014 Å when the torsion angle is lower. In the anion too, obtained on reduction, there is again a larger change in the bond 8, which is as much as 0.02 Å when the torsion angle is reduced. This could be due to the smaller angle subtended by the naphthalene groups with the anthracene and thereby conjugation increase reduces the bond order. On the other hand, the changes in the bond length of naphthalene groups on oxidation/reduction is hardly noticeable whereas there are substantial changes in the bond lengths in the anthracene moiety. It is interesting to note that there is no bond length alteration (BLA) in the side groups even when ϕ takes up lower angles but the larger BLA

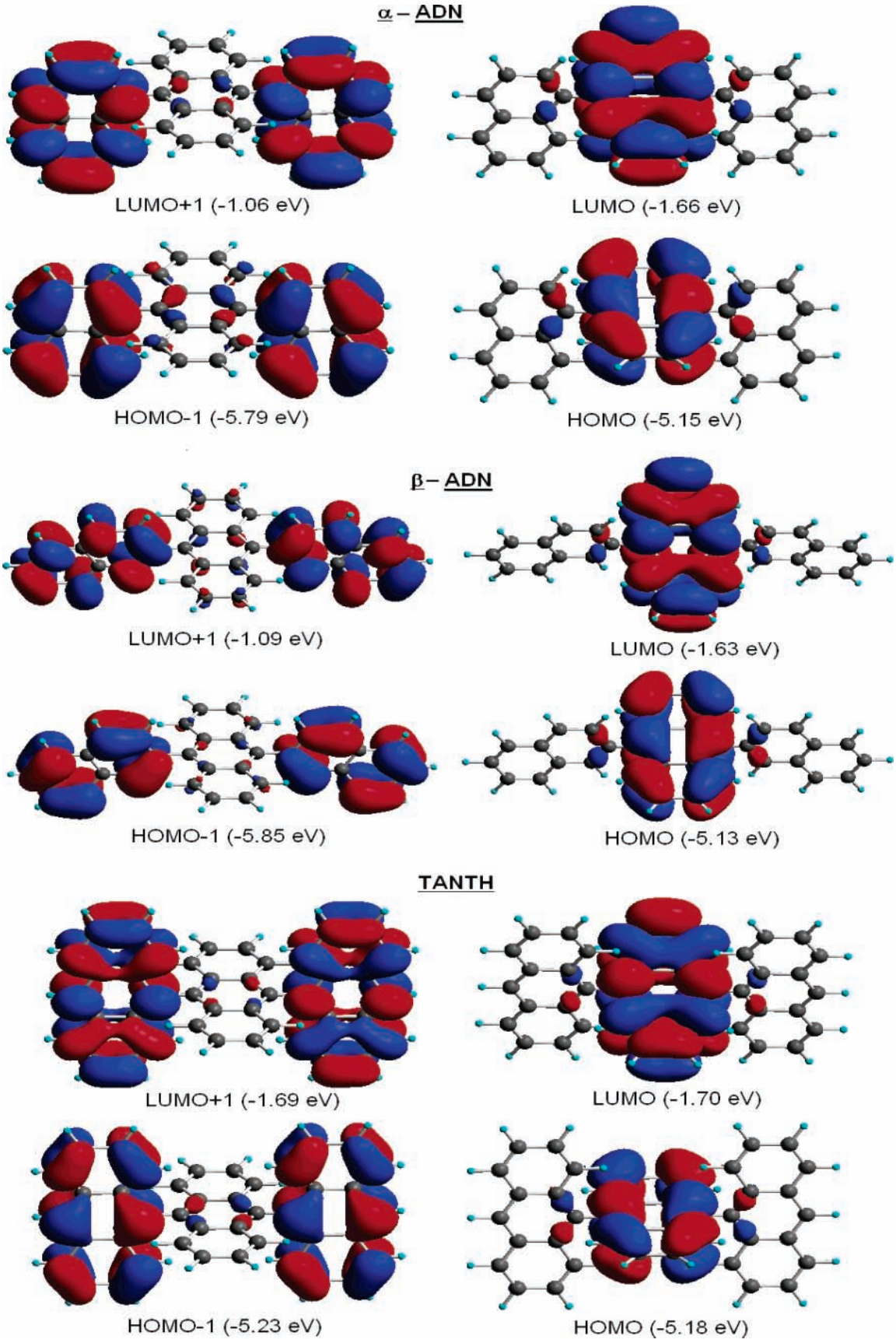

Figure 5. Frontier molecular orbital pictures of α-ADN, *β*-ADN and TANTH obtained for the B3LYP/6-31G(d,p) optimized structure.

again is seen only in the center anthracene. The changes in the substituted anthracene ring are comparable to that of the unsubstituted ring when the torsion angle is at 90°. Examining the BLA behavior in TANTH, one sees that the changes upon oxidation/reduction are much smaller. The maximum BLA is only 0.01 Å. In contrast to the ADN derivatives, here it is the side rings that show BLA and not the central ring. The connecting bond 8 also has much smaller changes.

(3) HOMO, LUMO Levels and HOMO−LUMO Gap (HLG). Next we investigate the changes that take place upon substitution, to the frontier orbitals, like the HOMO and LUMO energy levels, HOMO−LUMO gap, etc., in these anthracene derivatives. The calculated HOMO and the LUMO levels of all the molecules are shown in Table 4. The HOMO and the LUMO energies of anthracene lie at −5.22 and −1.63 eV, respectively, and a reasonably large HLG of 3.59 eV is obtained. Unsubstituted anthracene has the largest HLG in the series. By substituting groups at the 9 and 10 position there are no notable changes in the orbital densities (Figure 5) and the orbital contribution is still from the central anthracene as in the case of unsubstituted anthracene. On the other hand the energy levels change and in the case of α,*β*-ADN, the HOMO is slightly destabilized whereas the LUMO is slightly stabilized with the net result of a slightly smaller HLG. The HLG is now 3.49 eV compared to anthracene's 3.59 eV. The HOMOs of α-ADN and *β*-ADN lie almost at the same level, and they are around −5.10 and −5.15 eV. In the case of the LUMO they are around −1.65 and −1.66 eV, with a very minor difference of only 0.01 eV. On alkyl substitution on these molecules there is a further destabilization of the HOMO and the levels are now at −4.91 and at −4.88 eV. A destabilization is also seen in the case of the LUMOs, both of which are now at −1.4 eV. The HLG is almost equal in both α- and *β*-TMADN, which apparently has not changed from α,*β*-ADN upon substitution. The destabilization of the HOMO and the stabilization of the LUMO with respect to the unsubstituted anthracene is a maximum in TANTH and the HLG is 3.48 eV, about 0.02 eV smaller than the other HLG. Only a very small variation of 3.48−3.50 eV is observed in these substituted anthracenes.

The HOMO and the LUMO orbitals of the α- and *β*-ADN are shown in Figure 5. The HOMO is distributed along the main axis of the molecule with large densities on the vertex atoms, whereas the LUMO is more delocalized on the molecule. The HOMO−1 and the LUMO+1 of all the molecules shown in the figure lie on the side groups. HOMO and the HOMO−1 have an energy difference of 0.7 eV and about 0.6 eV in the case of LUMO and LUMO+1 in α- and *β*-ADN. But in TANTH these orbitals are almost degenerate indicating a deviation from the above trend. To understand the behavior of the HOMO, LUMO and the HLG with respect to ϕ, we carry out the variation of the angle vs these parameters and this is shown in Figure 6 only for α- and *β*-TMADN. The variation of the HOMO is smaller with change in angles but the LUMO stabilizes faster with a decrease in the angle. The HLG almost follows the similar behavior of the LUMO. In the α isomer, data below 35° are not possible due to steric factors. From this it can be understood that close packing with a large decrease in the rotation angle would reduce the HLG and thus the emission would no longer be in the blue. As the LUMO level changes with the rotated angle, small changes in the angle affects the electron injection and not the hole injection into the EL layer. The role of the bulky alkyl substitutions on the anthracene ring could be to hinder close packing in the solid state and allow the naphthyl groups to adopt the gas-phase optimal angle, which is ideal for emission in the blue. The calculated HOMO−LUMO data are in good agreement with the experimental data where both the α- and *β*-ADN derivatives are predicted to have the same HOMO and LUMO levels.[19] We can also infer from both the experimental data and the theoretical data that the larger dihedral angle would be taken up by the molecules in the solid state.

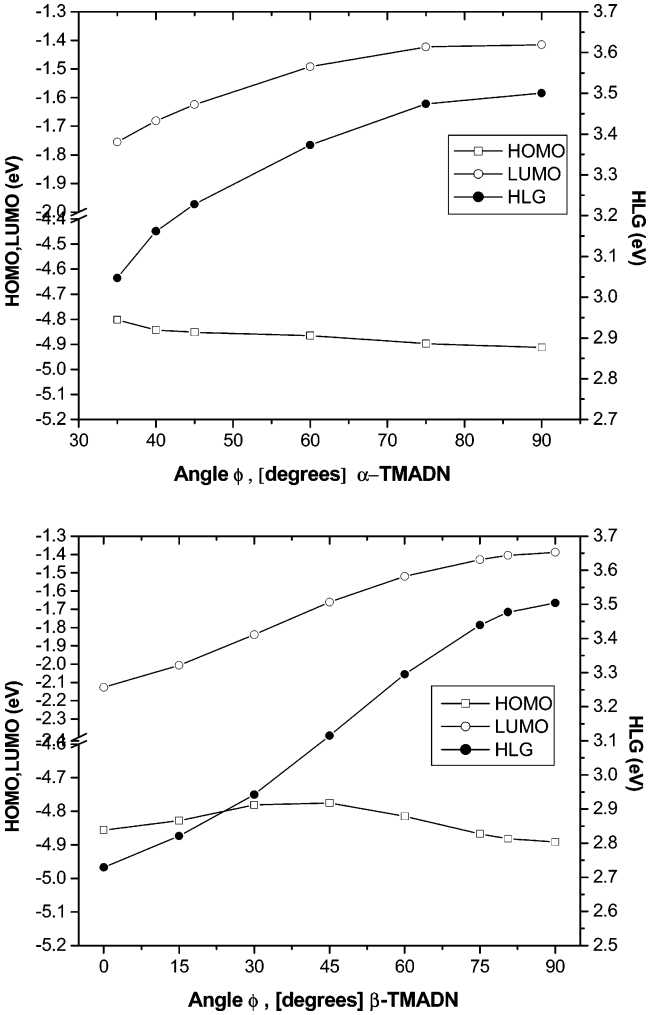

Figure 6. Effect of twisted dihedral angle (ϕ) on HOMO, LUMO and HLG in α-TMADN and *β*-TMADN molecules. Values obtained from B3LYP/6-31G(d,p) calculations.

(4) Electronic Absorption and Emission Spectra. The absorption and the emission spectra details calculated for all the molecules at their minima are shown in Table 4, and these are in good agreement with the experimental data where available.[16−21] In the unsubstituted anthracene the absorption maxima is around 379 nm. The major transition is from the HOMO to the LUMO. On substituting the 9 and 10 positions with naphthyl groups a red shift of around 20 nm in general is seen. The absorption is around 394 nm in the α-ADN with a slight red shift of only 6 nm in the case of the *β* isomer. In both isomers of TMADN and in TBADN the absorption is almost the same and it can be inferred that the changes in the absorption due to the alkyl substitutions are almost absent. But what is very interesting is that the oscillator strengths for the α isomers are always smaller than the *β* ones, whereas in the unsubstituted anthracene it is relatively very small. The reason for the lower oscillator strength in the case of the α isomers is due to the smaller polarization as seen from the transition dipole moments in the same table. To understand whether the angle plays any role in the increase or decrease of the absorption, we studied the variation of ϕ vs ΔE and f for both the α- and *β*-TMADN. This is shown in Figure 7. In the case of the α isomer (Figure 7a) the ΔE decreases with the angle. The oscillator strength increases till an angle of 45° to the value of 0.2 and then falls. The lowest ΔE value obtained is at an angle of 35°. Any lower angle than this is not possible due to steric

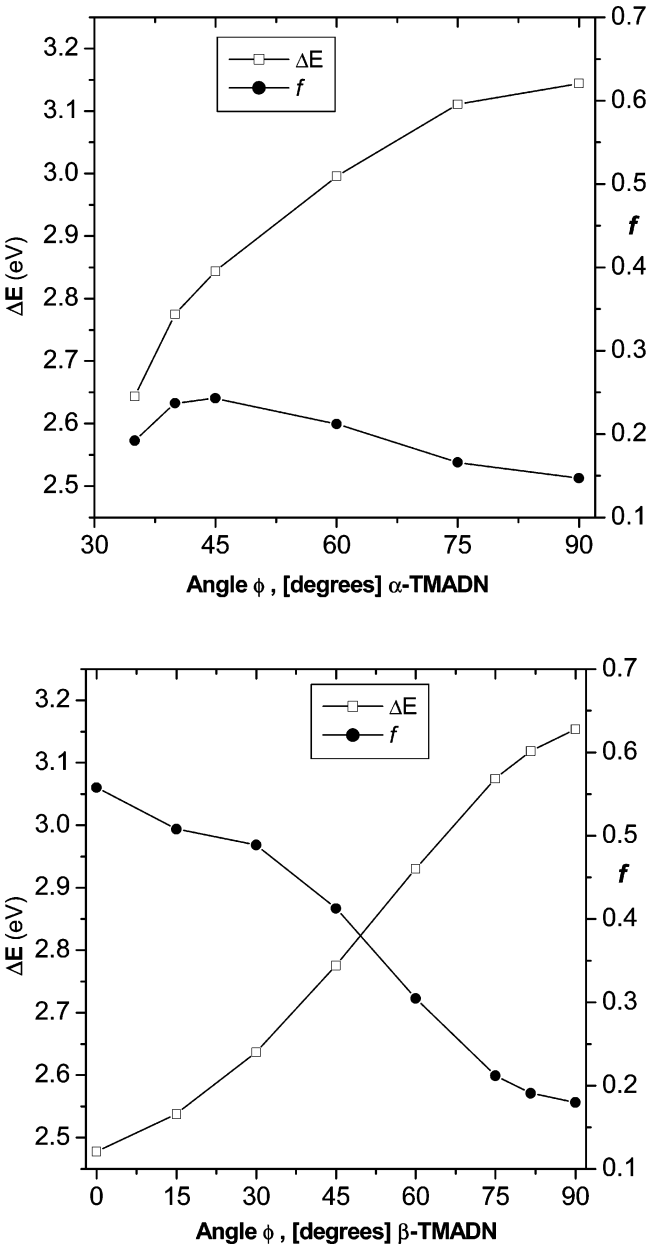

Figure 7. Effect of twisted dihedral angle (ϕ) on absorption energy (ΔE, eV) and oscillator strength (f) in α-TMADN and β-TMADN molecules. Values obtained from TD-B3LYP/6-31G(d,p) calculations.

hindrances. In the case of the β isomer, decreasing the angle decreases the ΔE while the oscillator strength increases. Thus at 0.0° the value of ΔE is less than 2.5 eV and f is at 0.6. From the tables it is seen that the absorption in the case of TANTH is slightly red shifted and has a larger oscillator strength.

The emission spectra details are shown in Table 5. The experimental results, which are available in the literature, are shown in the last column. The anthracene emission is calculated to be around 426 nm, whereas all other substituted anthracenes studied here emit above 440 nm. The α-TMADN has an emission maximum at 466 nm as determined experimentally and this is to be compared with 444 nm obtained here. β-TMADN has an experimental emission maximum also at 466 nm, whereas the calculated value is 443 nm. Basically, all these are LUMO to HOMO transitions. The intensities of the β isomer are again marginally stronger than in the α isomer. Here too TANTH has a slightly red shifted emission with a larger intensity.

TABLE 5: Wavelength (λ_{max} Emission, nm), Emission Energies (ΔE, eV), Oscillator Strength (f), Contributing Transitions and Transition Dipole Moments (Debye) for All Molecules Calculated Using TD-DFT for the CIS/6-31G(d,p) Optimized Geometries

molecule	λ_{max} emission (nm)	ΔE (eV)	f	transition	transition dipole (D)
anthracene	426 (420)[a]	2.91	0.06	L → H (0.62) L+1→ H−1 (0.11)	0.93
α-ADN[b]	444	2.79	0.17	L → H (0.62)	1.56
β-ADN[b]	442 (460)[a]	2.80	0.20	L → H (0.62)	1.71
α-TMADN[b]	444 (466)[a]	2.79	0.14	L → H (0.63)	1.45
β-TMADN[b]	443 (466)[a]	2.80	0.17	L → H (0.63)	1.59
β-TBADN[b]	443 (441)[a]	2.80	0.22	L → H (0.63)	1.79
DPA	441	2.81	0.14	L → H (0.62)	1.44
TANTH	445	2.79	0.22	L → H (0.62)	1.79

[a] Experimental values.[16−19] [b] Syn conformation only.

The ground-state dipole moments are shown in Table 4 and here the TBADN has the largest dipole moment of 0.53 D whereas the α and the β-TMADN have a very small dipole moment of 0.05 D. In both anthracene and α-ADN due to symmetry the dipole is absent.

(5) Hole/Electron Transport Properties and Transfer Integrals. Two widely used theories for describing the charge mobilities in organic materials are namely the band theory[13] and the hopping model.[34] With the overlap of neighboring molecules MO's the band is formed through which the conduction of the charge takes place according to the band theory model. On the other hand the hopping model is more suitable where coupling between neighboring molecule are small, and this is more appropriate in our case here. Using this model, the charge transport that is calculated here is the intermolecular process in which the charge hops between two molecules. The hole and electron transport process at the molecular level in the EL layer can then be portrayed as the electron transfer/hole transfer reactions between the neighboring molecules.[34−39]

$$\mathbf{A}^{+/\bullet} + \mathrm{A}' \rightarrow \mathrm{A}' + \mathrm{A}^{+/\bullet}$$

where A′ is the neutral molecule interacting with neighboring oxidized or reduced $A^{+/-}$. In the case of electron transport the interaction can be considered between a molecule in the neutral state interacting with a radical anion and in the case of hole transport the interaction can be considered between a molecule in the neutral state and a cation. The rate constant for electron transfer can be defined using the Marcus theory,[37]

$$K_{et} = 4\pi t^2/h(\pi/\lambda_{\pm}k_bT)^{1/2} \exp(-\lambda_{\pm}/4k_bT)$$

where t is the transfer integral/coupling matrix element between neighboring molecules, $\lambda_{\pm}$ is the reorganization energy, k_B is the Boltzmann constant and T is the temperature. An evaluation of t would require the relative positions of the molecules in the solid state as it is related to the energetic splitting of the frontier orbitals of the interacting molecules. On the other hand the mobilities of the electron/hole are predictable from the reorganization energies and in general have good agreement with the experimental observations.[34−39] Our aim here is to predict on the basis of the theoretical calculations the reorganization energy. It is clear that, to have larger hole/electron transport, the reorganization energy of the corresponding change from neutral to cation/neutral to anion should be low.

The reorganization energies are calculated on the basis of the model shown in Scheme 2. This model has been applied with success in many earlier studies.[6] Here the energy required

SCHEME 2: Calculation of the Reorganization Energy

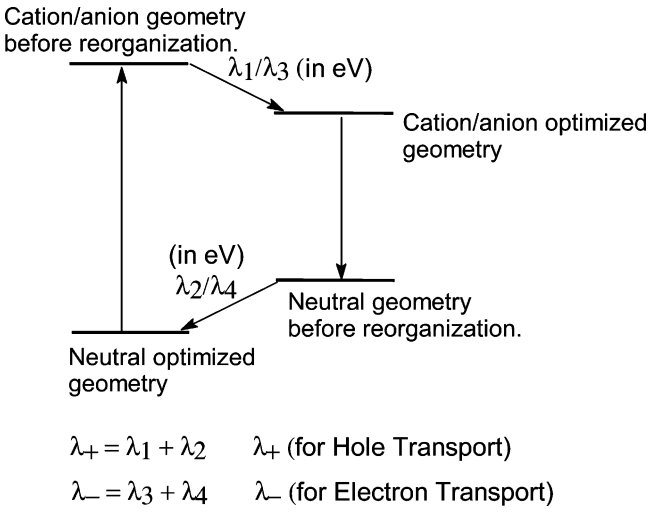

TABLE 6: Theoretical Estimation of the Reorganization Energies (eV) of All Molecules Obtained at the B3LYP/ 6-31G(d,p) Level for Case I, Where the Cation and Anion Have No Change in ϕ

molecule	λ_1	λ_2	λ_+	λ_3	λ_4	λ_-
benzene[a]	0.153	0.149	**0.302**	0.201	0.202	**0.403**
napthalene[a]	0.092	0.092	**0.184**	0.129	0.129	**0.258**
anthracene[a]	0.068	0.068	**0.136**	0.097	0.097	**0.194**
DPA	0.072	0.062	**0.134**	0.100	0.098	**0.198**
α-ADN	0.070	0.068	**0.138**	0.102	0.090	**0.192**
β-ADN	0.071	0.073	**0.144**	0.099	0.101	**0.200**
α-TMADN	0.068	0.068	**0.136**	0.107	0.087	**0.194**
β-TMADN	0.069	0.070	**0.139**	0.105	0.104	**0.209**
TANTH	0.020	0.020	**0.040**	0.040	0.028	**0.068**

[a] No dihedral angle in these cases.

(λ_1, eV) for the reorganization of the neutral geometry to the cation geometry upon removal of an electron added to the energy required (λ_2) to reorganize the obtained cation geometry back to a neutral state upon re-accepting an electron gives the total reorganization energy (λ_+) of the molecule when the charge is being transported. In a similar fashion the reorganization energy (λ_-) of the neutral to anion (λ_3) and back (λ_4) should be useful in understanding the electron transport.

In the calculation of the reorganization energies we could think of two possibilities here. In the first case as the 90° angle is the local minima for all the three neutral, cation and anion the reorganization takes place without the rotation of the side groups. For such a case the reorganization energies (in electronvolts) are shown in Table 6. For comparison the reorganization energies of benzene, naphthalene and anthracene are also shown in the same table. Values calculated for these molecules are in very good agreement with earlier reports.[40−42] As expected, in most of the cases the hole transport requires less reorganization energy than the electron transport. As the size of the molecule increases, there is in general a decrease in the reorganization energy. Hence of benzene, naphthalene and anthracene the lowest is for anthracene. It is seen that the hole transport is very good in anthracene as it requires a reorganization energy of 0.136 eV. α,β-ADN and TMADN almost have the same reorganization energy. The variation with respect to the unsubstituted anthracene is hardly 0.003 eV. This behavior is seen in electron transport also, whereas only in β-TMADN is the energy difference slightly larger. Thus the side groups largely do not perturb the hole and electron transport properties of the anthracene ring as long as the dihedral angle of the neutral molecule remains in the range. But in the case of TANTH there is an interesting deviation from this behavior. There is a large drop in the reorganization energy, it comes down to 0.040 eV for the hole transport compared to 0.136 eV of the unsubstituted anthracene. In the case of electron transport too it drops to 0.068 from 0.194 eV. Here, in general, λ_1 is equal to λ_2 and λ_3 is equal λ_4. This is because the geometry changes from neutral to cation/anion and vice versa are equal.

TABLE 7: Theoretical Estimation of the Reorganization Energies (eV) of All Molecules Obtained at the B3LYP/ 6-31G(d,p) Level for Case 2, Where the Cation and Anion Have Relaxed ϕ

molecule	λ_1	λ_2	λ_+	λ_3	λ_4	λ_-
DPA	0.151	0.12	**0.271**	0.155	0.148	**0.303**
α-ADN	0.125	0.137	**0.262**	0.117	0.146	**0.263**
β-ADN	0.222	0.135	**0.357**	0.286	0.179	**0.465**
α-TMADN	0.087	0.104	**0.191**	0.135	0.150	**0.285**
β-TMADN	0.165	0.115	**0.280**	0.318	0.186	**0.504**
β-TBADN	0.175	0.139	**0.314**	0.213	0.183	**0.396**
TANTH	0.055	0.081	**0.136**	0.055	0.053	**0.108**

There is a second possibility in which the cation/anion geometry could relax to the lower minima, i.e., the smaller dihedral angle. The reorganization energies calculated for such a geometry relaxation would be different from the one discussed earlier. The values are tabulated in Table 7. Here the rotation angle in the cation and anion being smaller, larger changes are seen. The hole transport in general goes through a larger reorganization energy change. The values are as high as 0.357 eV and the lowest is 0.191 eV, which is still larger than those in Table 6. In the case of electron transport the difference is still higher. In fact, for β-TMADN the value is as high as 0.504 eV. Such large reorganization energies can be compared with those molecules such as (4-biphenylphenyl)-*m*-tolyamine (0.50 eV), 4,4′-bis(phenyl-*m*-tolylamino)biphenyl (0.56 eV) and 4,4′-diaminobiphenyl with the amine group taken as pyramidal (0.67 eV). All these molecules have a fairly large rotational freedom and on oxidation and reduction they undergo large geometry change.[34a] Unlike case 1, we find that in general λ_1 is not equal to λ_2 and in electron transport λ_3 is not equal to λ_4. This is because the geometry changes from neutral to cation/anion and vice versa are not the same. Similar cases have been reported in earlier studies.[34a]

The transfer integrals, *t*, can be calculated using the direct coupling scheme or Koopman's theorem.[43,44] The distance *r* between the centers of anthracene moieties in this case are quite large (minimum distance of 6.0 Å) due to the bulky side groups that do not allow any closer packing. In an earlier study it was seen that at larger distances Koopman's theorem performs well and the results are almost the same as that obtained by the two state model.[45] Keeping these points in view, we have used Koopman's theorem method. The splittings are calculated using the energies of the HOMO, HOMO−1, LUMO and LUMO +1 of the dimers,[46] which have been obtained with the INDO Hamiltonian at the DFT/B3LYP optimized geometry. The energy difference of the HOMO and HOMO−1 gives the energy splitting for the hole transport whereas the LUMO and LUMO+1 difference gives the energy splitting of the electron transport. As we do not have the solid-state experimental data and the number of possible orientations of two molecules interacting with each other is quite large, we restrict our study of the transfer integral to only two orientations in co-facial arrangement with ϕ at 90°. This is only to compare the splitting patterns in the two isomers. These are shown in Figures 8 and 9. Here (Figure 8) the α isomer interacts in a co-facial manner with another α isomer with the long end of the naphthalene on

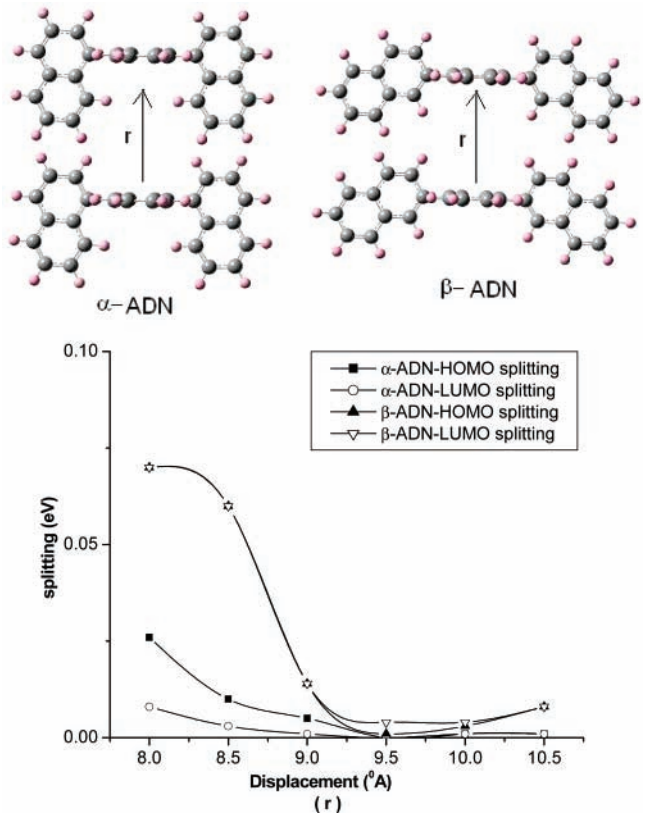

Figure 8. Energy splitting as a function of the distance, *r*, in the cofacial arrangement of the dimer with the long sides of naphthalene oriented in the same direction.

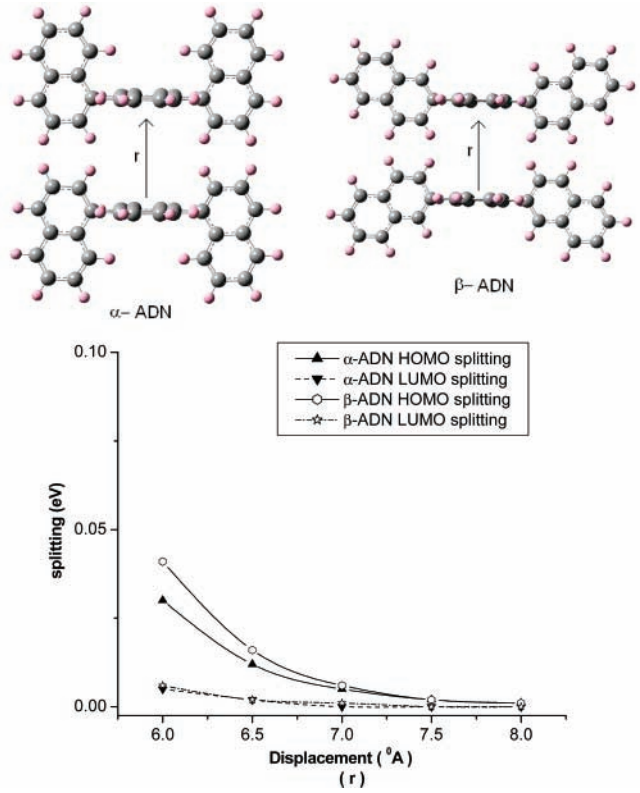

Figure 9. Energy splitting as a function of the distance, *r*, in the cofacial arrangement of the dimer with the longer sides of naphthalene on the opposite side.

the same side. For comparison in the same graph the values of the β isomers are also shown. In the other figure (Figure 9) the α isomer interacts with another isomer with the short ends of the naphthalene facing each other. Here again the β isomer is shown for comparison. At the first instance it is seen that in all the graphs the coupling is 1 order of magnitude less than the parent anthracene due to larger *r*. In the case where the short ends face each other (Figure 9), we find that the transfer integrals are almost same for both the α and the β isomer. But in the other case (Figure 8) we see that the β isomer has a much larger coupling than the α isomer. Thus the larger reorganization energy of the β isomer and different type of coupling between adjacent molecules in the α and β isomers, suggests that mixtures might show different efficiency than the individual isomers as observed by Kan et al.[19]

Conclusions

The side groups, in 9,10-bis(1-naphthyl)anthracene (α-ADN) and 9,10-bis(2-naphthyl)anthracene (β-ADN) isomers and in their derivatives, have a low energy of rotation for a particular range near the equilibrium geometry. The β isomer has a larger range than the α isomer due to less steric interactions. Irrespective of the angle in this range, it is noticed that properties such as the BLA, absorption, emission and also the HOMO−LUMO gap remain the same. From the geometry it is seen that the α isomer cannot adopt a planar structure due to steric hindrance whereas the β isomer requires very high energy for the planar structure. Properties calculated at large angles are in good agreement with the experimental data. Upon oxidation/reduction the BLA takes place only in the anthracene ring and not in the side rings.

Calculation of the reorganization energy, to estimate the hole and the electron transport reveals that the β isomer has lower hole/electron transport, with nearly a factor of 1.5−2.0 times more reorganization energy than that of the α isomer. On the other hand when there is no change in the dihedral angle upon oxidation/reduction the hole and electron transport remains almost the same as in the unsubstituted anthracene. The transfer integrals indicate that in some conformations the β isomer has larger values than the α isomer hence more coupling between the neighboring molecules. In general, the values are almost 1 order of magnitude less than that observed in unsubstituted anthracene.

The holes accumulate in the EL layer because the HOMOs of the EL layer and the ET layer have a large energy difference and hence mobility in the interlayer becomes difficult. On the other hand, the LUMO levels of the ET layer and the EL layer match very well so there is a flow of electrons into the EL layer. Larger reorganization energy at this stage for the electron/hole transport in the EL layer favors a higher recombination of the holes and electrons in the EL layer thereby increasing the efficiency. To put it another way, the EL layer acts as both the hole and electron trap. The above calculations are in very good agreement with the experimental observations.

Finally, studies on 9,10-dianthrylanthracene as a possible candidate for the EL layer reveals that the properties are no longer the same as in naphthyl derivatives. There is a smaller reorganization energy for both hole and electron transport and this may not yield the same efficiency.

Acknowledgment. We thank the Director, IICT and the Head, Inorganic Chemistry division, IICT, for their constant encouragement in this work. P.R. thanks CSIR for the SRF, and M.A.R. thanks UGC for the JRF fellowship.

References and Notes

(1) Friend, R. H.; Gymer, R. W.; Holmes, A. B.; Burroughes, J. H.; Marks, R. N.; Taliani, C.; Bradley, D. D. C.; Dos Santos, D. A.; Bredas, J.

L.; Logdlund, M.; Salaneck, W. R. *Nature* **1999**, *397*, 121−128.
(2) Mitschke, U.; Bauerle, P. *J. Mater. Chem.* **2000**, *10*, 1471−1507.
(3) Hung, L. S.; Chen, C. H. *Mater. Sci. Eng.* **2002**, *39*, 143−222.
(4) Dini, D. *Chem. Mater.* **2005**, *17*, 1933−1945.
(5) Aziz, H.; Popovic, Z. D. *Chem. Mater.* **2004**, *16*, 4522−4532.
(6) Bredas, J. L.; Beljonne, D.; Coropceanu, V.; Cornil, J.; *Chem. Rev.* **2004**, *104*, 4971−5003.
(7) Cornil, J.; Beljonne, D.; Calbert, J. P.; Bredas, J. L. *Adv. Mater.* **2001**, *13*, 1053−1067.
(8) Tretiak, S.; Mukamel, S. *Chem. Rev.* **2002**, *102*, 3171−3212.
(9) Bredas, J. L. *Adv. Mater.* **1995**, *7*, 263−274.
(10) Risko, C.; Kushto, G. P.; Kafafi, Z. H.; Bredas, J. L. *J. Chem. Phys.* **2004**, *121*, 9031−9038.
(11) Bredas, J. L.; Cornil, J.; Beljonne, D.; Santos, D. D.; Shuai, Z. *Acc. Chem. Res.* **1999**, *32*, 267−276.
(12) Kwon, O.; Coropceanu, V.; Gruhn, N. E.; Durivage, J. C.; Laquindanum, J. G.; Katz, H. E.; Cornil, J.; Bredas, J. L. *J. Chem. Phys.* **2004**, *120*, 8186−8194.
(13) (a) Bredas, J. L.; Calbert, J. P.; da Silva Filho, D. A.; Cornil, J. *Proc. Natl. Acad. Sci. U.S.A.* **2002**, *99*, 5804−5809. (b) Cheng, Y. C.; Silbey, R. J.; da Silva Filho, D. A.; Calbert, J. P.; Cormil, J.; Bredas, J. L. *Chem. Phys.* **2003**, *118*, 3764.
(14) da Silva Filho, D. A.; Kim, E. G.; Bredas, J. L. *Adv. Mater.* **2005**, *17*, 1072−1076.
(15) Garcıa, J. C. S.; Bredas, J. L.; Beljonne, D.; Cornil, J.; Alvarez, R. M.; Hanack, M.; Poulsen, L.; Gierschner, J.; Mack, H. G.; Egelhaaf, H. J.; Oelkrug, D. *J. Phys. Chem. B* **2005**, *109*, 4872−4880.
(16) Shi, J.; Tang, C. W. *Appl. Phys. Lett.* **2002**, *80*, 3201−3203.
(17) Kan, Y.; Wang, L.; Gao, Y.; Duan, L.; Wu, G.; Qiu, Y. *Synth. Met.* **2004**, *141* 245−249.
(18) Tao, S.; Hong, Z.; Peng, Z.; Ju, W.; Zhang, X.; Wang, P.; Wu, S.; Lee, S. *Chem. Phys. Lett.* **2004**, *397*, 1−4.
(19) Kan, Y.; Wang, L.; Duan, L.; Hu, Y.; Wu, G.; Qiu, Y. *Appl. Phys. Lett.* **2004**, *84*, 1513−1515.
(20) (a) Lee, M. T.; Chen, H. H.; Liao, C. H.; Tsai, C. H.; Chen, C. H. *Appl. Phys. Lett.* **2004**, *85*, 3301−3303. (b) Liu, T. H.; Wu, Y. S.; Lee, M. T.; Chen, H. H.; Liao, C. H.; Chen, C. H. *Appl. Phys. Lett.* **2004**, *85*, 4304−4306.
(21) (a) Cao, W.; Zhang, X.; Bard, A. J. *J. Electroanal. Chem.* **2004**, *566*, 409−413. (b) Zheng, S.; Shi, J. *Chem. Mater.* **2001**, *13*, 4405. (c) Li, Y.; Fung, M. K.; Xie, Z.; Lee, S.-T.; Hung, L. S.; Shi, J. *Adv. Mater.* **2002**, *14*, 1317. (d) Zhang, X. H.; Liu, M. W.; Wong, O. Y.; Lee, C. S.; Kwong, H. L.; Lee, S. T.; Wu, S. K. *Chem. Phys. Lett.* **2003**, *369*, 478. (e) Hsu, S. F.; Lee, C. C.; Hu, A. T.; Chen, C. H. *Curr. Appl. Phys.* **2004**, *4*, 663−666.
(22) Fang, Y.; Gao, S.; Yang, X.; Shuai, Z.; Beljonne, D.; Bredas, J. L. *Synth. Met.* **2004**, *141*, 43−49.
(23) Fang, H. H.; So, S. K.; Sham, W. Y.; Lo, C. F.; Wu, Y. S.; Chen, C. H. *Chem. Phys.* **2004**, *298*, 119−123.
(24) Frisch, M. J.; Trucks, G. W.; Schlegel, H. B.; Scuseria, G. E.; Robb, M. A.; Cheeseman, J. R.; Montgomery, J. A., Jr.; Vreven, T.; Kudin, K. N.; Burant, J. C.; Millam, J. M.; Iyengar, S. S.; Tomasi, J.; Barone, V.; Mennucci, B.; Cossi, M.; Scalmani, G.; Rega, N.; Petersson, G. A.; Nakatsuji, H.; Hada, M.; Ehara, M.; Toyota, K.; Fukuda, R.; Hasegawa, J.; Ishida, M.; Nakajima, T.; Honda, Y.; Kitao, O.; Nakai, H.; Klene, M.; Li, X.; Knox, J. E.; Hratchian, H. P.; Cross, J. B.; Bakken, V.; Adamo, C.; Jaramillo, J.; Gomperts, R.; Stratmann, R. E.; Yazyev, O.; Austin, A. J.; Cammi, R.; Pomelli, C.; Ochterski, J. W.; Ayala, P. Y.; Morokuma, K.; Voth, G. A.; Salvador, P.; Dannenberg, J. J.; Zakrzewski, V. G.; Dapprich, S.; Daniels, A. D.; Strain, M. C.; Farkas, O.; Malick, D. K.; Rabuck, A. D.; Raghavachari, K.; Foresman, J. B.; Ortiz, J. V.; Cui, Q.; Baboul, A. G.; Clifford, S.; Cioslowski, J.; Stefanov, B. B.; Liu, G.; Liashenko, A.; Piskorz, P.; Komaromi, I.; Martin, R. L.; Fox, D. J.; Keith, T.; Al-Laham, M. A.; Peng, C. Y.; Nanayakkara, A.; Challacombe, M.; Gill, P. M. W.; Johnson, B.; Chen, W.; Wong, M. W.; Gonzalez, C.; Pople, J. A. *Gaussian 03*, revision C.02; Gaussian, Inc.: Wallingford, CT, 2004.
(25) Becke, A. D. *Phys. Rev. A* **1988**, *38*, 3098−3100; *J. Chem. Phys.* **1993**, *98*, 5648−5652.
(26) Lee, C.; Yang, W.; Parr, R. G. *Phys. Rev. B* **1988**, *37*, 785−789.
(27) Stratmann, R. E.; Scuseria, G. E.; Frisch, M. J. *J. Chem. Phys.* **1998**, *109*, 8218−8224.
(28) (a) Tozer, D. T.; Handy, N. C. *Phys. Chem. Chem. Phys.* **2000**, *2*, 2117. (b) Becke, A. D. *J. Chem. Phys.* **1996**, *104*, 1040. (c) Casida, M. E.; Jamorski, C.; Casida, K. C.; Salahub, d. R. *J. Chem. Phys.* **1998**, *108*, 4439.
(29) (a) Foresman, J. B.; Head-Gordon, M.; Pople, J. A.; Frisch, M. J. *J. Phys. Chem.* **1992**, *96*, 135−149. (b) Pople, J. A.; Beveridge, D.; Dobosh, P. *J. Chem. Phys.* **1967**, *47*, 2026.
(30) Teng, Y. L.; Kan, Y. H.; Su, Z. M.; Liao, Y. Yan, L.K.; Yang, Y. J.; Wang, R. S. *Int. J. Quantum Chem.* **2005**, *103*, 775.
(31) Sakata, K.; Hara, K. *Chem. Phys. Lett.* **2003**, *371*, 164.
(32) Adams, J. M.; Ramdas, S. *Acta Crystallogr. Sect. B* **1979**, *35*, 679.
(33) Langer, V.; Becker, H. D. *Z. Kristallogr.* **1992**, *199*, 313.
(34) (a) Lin, B. C.; Cheng, C. P.; Michael Lao, Z. P. *J. Phys. Chem. A* **2003**, *107*, 5241−5251. (b) Nelsen, S. F.; Trieber, D. A., II; Ismagilov, R. F.; Teki, Y. *J. Am. Chem. Soc.* **2001**, *123*, 5684. (c) Nelsen, S. F.; Blomgren, F. *J. Org. Chem.* **2001**, *66*, 6551. (d) Sakanoue, K.; Motoda, M.; Sugimoto, M.; Sakaki, S. *J. Phys. Chem. A* **1999**, *103*, 5551. (e) Malagoli, M.; Bredas, J. L. *Chem.* Phys. Lett. **2000**, *327*, 13. (f) Li, X.-Y.; Tong, J.; He, F.-C. *Chem. Phys.* **2000**, *260*, 283. (g) Marcus, R. A.; Sutin, N. *Biochim. Biophys. Acta* **1985**, *811*, 265.
(35) Barbara, P.; Meyer, T.; Ratner, M. *J. Phys. Chem.* **1996**, *100*, 13148−13168.
(36) Cornil, J.; Lemaur, V.; Calbert, J. P.; Bredas, J. L. *Adv. Mater.* **2002**, *14*, 726−729.
(37) Marcus, R. J. *J. Chem. Phys.* **1956**, *24*, 966−978.
(38) Lin, B. C.; Cheng, C. P.; You, Z.-Q.; Hsu, C.-P. *J. Am. Chem. Soc.* **2005**, *127*, 66−67.
(39) Deng, W. Q.; Goddard, W. A., III. *J. Phys. Chem. B* **2004**, *108*, 8614−8621.
(40) Coropceanu, V.; Malagoli, M.; da Silva Filho, D. A.; Gruhn, N. E.; Bill, T. G.; Bredas, J. L. *Phys. Rev. Lett.* **2002**, *89*, (275503), 1−4.
(41) Mason, R. *Acta Crystallogr.* **1964**, *17*, 547−555.
(42) Klimkans. A.; Larsson. S. *Chem. Phys.* **1994**, *189*, 25.
(43) You, Z.-Q.; Shao, Y.; Hsu, C.-P. *Chem. Phys. Lett.* **2004**, *390*, 116.
(44) (a) Ohta, K.; Closs, G. L.; Morokuma, K.; Green, N. J. *J. Am. Chem. Soc.* **1986**, *108*, 1319. (b) Farazdel, A.; Dupuis, M.; Clementi, E.; Aviram, A. *J. Am. Chem. Soc.* **1990**, *112*, 4206.
(45) Lu, S.-Z.; Li, X.-Y.; Liu, J.-F. *J. Phys. Chem. A* **2004**, *108*, 4125.
(46) (a) Li, X. Y.; Tang, X. S.; He, F. C. *Chem. Phys.* **1999**, *248*, 137. (b) Li, X. Y.; He, F. C. *J. Comput. Chem.* **1999**, *20*, 597.